*Int. J. Heat Mass Transfer.* Vol. 25, No. 10, pp. 1511–1522, 1982
Printed in Great Britain

0017-9310/82/101511-12 $03.00/0
Pergamon Press Ltd.

# THEORETICAL TREATMENT OF EVAPORATION FRONT DRYING

G. RONALD HADLEY
Sandia National Laboratories, Albuquerque, NM 87185, U.S.A.

(*Received* 17 *September* 1981 *and in final form* 19 *February* 1982)

**Abstract**—A general formalism is presented for the combined diffusion and forced flow of a binary gas mixture through a porous medium. The resulting equations are then specialized to handle the vapor region of a porous material which is drying according to a receding evaporation front model. Solutions presented for various permeabilities and temperatures give the conditions under which air is present in the pores and allow one to investigate the usefulness of the 'boiling' concept for the drying of low permeability materials. Evaporation front motion together with the water loss rate is examined for different curvilinear geometries both analytically and numerically.

## NOMENCLATURE

$C$, constant defined in equation (72);
$D_{ij}$, binary gaseous diffusion coefficient;
$D_{iK}$, Knudsen diffusion coefficient;
$J$, flux [number/(area × time)];
$k$, Boltzmann constant;
$k_{l,v}$, thermal conductivity;
$L$, latent heat of vaporization;
$l$, normalization length;
$m$, geometry indicator;
$m_{v,a}$, mass of gas molecule;
$n$, number density;
$p$, pressure;
$R$, mean pore radius;
$r$, position coordinate;
$S$, constant defined by equation (45);
$T$, temperature;
$t$, time;
$u$, evaporation front velocity;
$v$, mean gas velocity in axial direction;
$v^{th}$, thermal velocity;
$v_{1D}$, Darcy velocity, equations (24) and (25) only;
$X_i$, external force exerted on gas $i$ molecules;

Greek symbols

$\alpha$, thermal diffusivity;
$\gamma$, dimensionless constant defined by equation (67);
$\delta$, dimensionless constant defined by equation (92);
$\eta$, dimensionless constant defined by equation (37);
$\kappa$, permeability;
$\mu$, viscosity of gas mixture;
$\rho$, mass density;
$\xi$, dimensionless constant defined by equation (38);
$\phi$, porosity.

Subscripts

a, air;
amb, ambient (drying atmosphere);
f, evaporation front;
$i$, gas component 1 or 2;
K, Knudsen;
l, liquid;
0, reference condition;
v, vapor;
vap, equilibrium vapor.

Superscripts

th, thermal;
$'$, quantity evaluated in moving coordinate system;
$\bar{}$, averaged over pore diameter;
$\tilde{}$, non-dimensional.

## 1. INTRODUCTION

WATER loss by evaporation from porous materials is an area of study which has many diverse applications. Early work in this area was concerned mostly with agricultural applications [1, 2] (drying of soils) and industrial applications in the field of chemical engineering [3]. More recent work has expanded to include the drying of concrete [4], and other molded materials [5]. Still another area of interest has opened up due to investigations of the use of geological formations as repositories for nuclear waste canisters [6]. In the latter case, heat generated by the waste canisters leads to drying of the surrounding rock.

Several decades of research in the area of drying of porous solids has led to the acceptance of two main theories of drying. In the first, movement of water takes place to the drying surface as the result of capillary forces acting within the pores. This kind of model has led to a 'diffusion' theory governed by a highly nonlinear diffusion equation [7], and has received considerable attention in the soil physics literature. In the second, water transport occurs as a vapor through a region of 'dry' material from a receding evaporation front. Usually the liquid or 'wet' region is taken as stationary, with front 'motion' occurring only due to

evaporation into the vapor phase. The latter model seems most applicable where water loss rates are high and capillary forces are not sufficient to smear out the front. Drying which takes place at elevated temperatures is one example where conditions are likely to favor the evaporation front model over the diffusion model. The remainder of this paper will concentrate exclusively on the evaporation front model.

The primary emphasis of the present paper is on a more complete treatment of the vapor region in an evaporation front drying process. Gupta [8] and Mikhailov [9] treat the front as being controlled by heat balance, in which case a detailed treatment of the vapor region is unnecessary. Such a model is only applicable in situations where the evaporation front is at a known temperature, or other information concerning the temperature profile is available. The calculation thus reduces essentially to a solution of the heat equation with latent heat effects included at the front position. Mikhailov [9] has also included a calculation in which the vapor flux is governed by Darcy's law, as have Cross *et al.* [10] and Hohlfelder and Hadley [6]. This treatment is shown below to be valid only within certain parameter regimes since it ignores binary gas effects such as diffusion as well as molecular effects which are important for materials with a small average pore size. In general, these refinements may not be ignored except in certain special cases which will be examined in detail below.

The theoretical treatment presented here is of sufficient generality to include most of the cases mentioned above. It does, however, necessitate some simplifying assumptions which are as follows:

(1) All effects arising from surface tension forces are excluded. All liquid water is assumed stationary.

(2) The porous medium is assumed to have a unimodal pore distribution, so that a well-defined average pore radius exists. The pore structure is modeled as straight capillary tubes.

(3) The vapor flux emanating from the evaporation front is sufficiently small so that the partial pressure of water vapor at the front is given by the equilibrium value.

(4) Both air and water vapor are treatable as ideal gases.

(5) All viscous flow is assumed to be laminar (obeying Darcy's law at high pressures).

(6) A sharply-defined evaporation front is assumed to separate a region of 100% saturation (all voids filled with liquid $H_2O$) from a region of zero saturation (all voids contain gases only).

(7) Vapor motion velocities are large compared with front velocities so that all vapor obeys the steady state continuity equation at any given time.

## 2. GENERAL VAPOR REGION EQUATIONS

The diffusion and flow of a mixture of gases through a porous medium is a very complex and difficult problem. The most thorough treatment of this problem appears to be the series of articles by Mason, Evans and Watson [11–13], culminating several years later in the paper by Mason, Malinauskas and Evans [14]. Although the transport equations derived in this section are essentially identical to those presented by Mason *et al.* [14], a thorough derivation is included herein for two reasons: (i) the result is obtained in a simpler manner than the previous development, and (ii) their additive relation for viscous effects is shown to arise naturally from a coordinate transformation.

Let us first consider the flow and diffusion of a binary gas system through a single capillary tube of fixed radius $R$. Hirschfelder, Curtiss and Bird [15] show that the momentum equation for such a mixture is identical to that for a single gas if the gas velocity is replaced by the mass average velocity of the mixture. Consequently we have for steady non-accelerating flow

$$\frac{\partial p}{\partial z} = \frac{\mu}{r}\frac{\partial}{\partial r}\left(r\frac{\partial v}{\partial r}\right) \tag{1}$$

where $z$ and $r$ are the axial and radial coordinate, respectively, $\mu$ is the mixture viscosity, and

$$v = \frac{m_1 n_1 v_1 + m_2 n_2 v_2}{m_1 n_1 + m_2 n_2} = \frac{\rho_1 v_1 + \rho_2 v_2}{\rho}. \tag{2}$$

The subscripts 1 and 2 refer to the component gases. The solution to equation (1) for $\partial p/\partial z$ constant is the well-known equation for Hagen–Poiseuille flow

$$v(r) = v_0 + \frac{r^2 - R^2}{4\mu}\frac{\partial p}{\partial z}. \tag{3}$$

The mean velocity is found by averaging equation (3) over the cross-section of the tube, and is

$$\bar{v} = v_0 - \frac{R^2}{8\mu}\frac{\partial p}{\partial z}. \tag{4}$$

The so-called 'slip velocity' $v_0$ arises from molecular interactions and is thus directly related to the phenomena of Knudsen diffusion and binary gaseous diffusion. The mass average velocity profile is shown in Fig. 1.

If we define

$$v_D \equiv -\frac{R^2}{8\mu}\frac{\partial p}{\partial z} \tag{5}$$

then equation (4) may be written

$$\bar{v} = v_0 + v_D. \tag{6}$$

The form of equation (6) suggests a transformation into a coordinate frame moving with velocity $v_D$ relative to the laboratory frame. Denoting quantities in the moving frame with primes, we have

$$\bar{v}' = \bar{v} - v_D = v_0, \tag{7}$$

that is, velocities in the primed frame are on the average due to molecular effects only. We may also decompose equation (6) into

$$\bar{v}_i = v_{i0} + v_D. \tag{8}$$

for each gas species since equation (8) may be regarded as the definition of $v_{i0}$. Note that combining equation (8) for both values of $i$ reproduces equation (6). In the primed frame we next apply the diffusion equation given in Hirschfelder *et al.* [15]

$$\frac{n_2J'_1 - n_1J'_2}{n^2D_{12}} = \frac{\partial}{\partial z}\left(\frac{p_1}{p}\right) + \left(\frac{p_1}{p} - \frac{n_1m_1}{\rho}\right) \times \frac{\partial \ln p}{\partial z} - \frac{n_1m_1}{p\rho}\left(\frac{\rho}{m_1}X'_1 - n_1X'_1 - n_2X'_2\right) \quad (9)$$

where $D_{12}$ is the binary diffusion coefficient between the two gases, $p_1$ is the partial pressure of gas 1, and $X_i$ is the external force/molecule exerted on gas $i$. Here we have neglected the thermodiffusion term and introduced the number fluxes $J'_i = n_iv'_i$, with $n_i$ the number density of gas $i$. In this case the only external forces are those exerted by the walls of the capillary tube due to collisions. Since Knudsen diffusion involves only gas–wall collisions, we may derive a form for the $X$'s by considering the Knudsen formula [16] for a single gas

$$J_{i0} = -\frac{D_{iK}}{kT}\frac{\partial p_i}{\partial z} \quad (10)$$

which has been generalized from [16] to include non-uniform temperature effects. Here $J_{i0}$ is the flux of molecules of gas $i$ relative to the wall, and $D_{iK}$ is the Knudsen diffusion coefficient

$$D_{iK} = \frac{2}{3}Rv_i^{th} \quad (11)$$

with

$$v_i^{th} = \left(\frac{8kT}{\pi m_i}\right)^{1/2}. \quad (12)$$

Balancing forces on a cylinder of gas $i$ then gives

$$X_i = \frac{1}{n_i}\frac{\partial p_i}{\partial z} = -\frac{kTJ_{i0}}{n_iD_{iK}}. \quad (13)$$

In order to apply equation (13) to the mixture problem at hand, we need the flux of gas $i$ relative to the wall expressed in primed variables. From equations (7) and (8) we obtain

$$J_{i0} = J'_{i0} + n_iv_D = (J'_i - n_iv_D) + n_iv_D = J'_i. \quad (14)$$

Inserting equations (13) and (14) into equation (9) gives

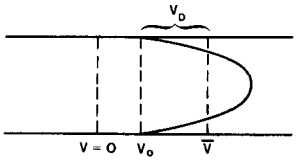


FIG. 1. Mass average velocity profile for flow through a capillary tube.

$$\frac{n_2J'_1 - n_1J'_2}{n^2D_{12}} = \frac{1}{p}\frac{\partial p_1}{\partial z} + \frac{kT}{pD_{1K}}J'_1 - \frac{n_1m_1}{p\rho}\left[\frac{\partial p}{\partial z} - n_1X'_1 - n_2X'_2\right]. \quad (15)$$

The term in brackets is zero since without viscous effects (in the primed frame) the net pressure gradient must balance the total force exerted by the wall. Consequently equation (15) may be rearranged to read

$$J'_1 = -\frac{D_{1K}}{kT}\frac{\partial p_1}{\partial z} + \frac{D_{1K}}{nD_{12}}(n_2J'_1 - n_1J'_2). \quad (16)$$

Applying the transformation (7) back into the lab frame then gives

$$J_1 = -\frac{D_{1K}}{kT}\frac{\partial p_1}{\partial z} - \frac{n_1R^2}{8\mu}\frac{\partial p}{\partial z} + \frac{D_{1K}}{nD_{12}}(n_2J_1 - n_1J_2). \quad (17)$$

The companion equation to equation (17) may be obtained by interchanging indices since the gases are formally equivalent

$$J_2 = -\frac{D_{2K}}{kT}\frac{\partial p_2}{\partial z} - \frac{n_2R^2}{8\mu}\frac{\partial p}{\partial z} + \frac{D_{2K}}{nD_{12}}(n_1J_2 - n_2J_1). \quad (18)$$

Equations for a porous medium may be obtained from equations (17) and (18) by multiplying through by $\phi$ and defining

$$J_{ip} = \phi J_i \quad (19)$$

and

$$\kappa = \frac{\phi R^2}{8}.$$

Omitting the subscript $p$ for clarity, the final equations are then

$$J_1 = -\frac{\phi D_{1K}}{kT}\frac{\partial p_1}{\partial z} - \frac{n_1\kappa}{\mu}\frac{\partial p}{\partial z} + \frac{D_{1K}}{nD_{12}}(n_1J_2 - n_2J_1) \quad (20)$$

and

$$J_2 = -\frac{\phi D_{2K}}{kT}\frac{\partial p_2}{\partial z} - \frac{n_2\kappa}{\mu}\frac{\partial p}{\partial z} + \frac{D_{2K}}{nD_{12}}(n_2J_1 - n_1J_2) \quad (21)$$

where now the $J$'s are 'filtration' fluxes, i.e. averaged over the porous material. Note that equations (20) and (21) are consistent with the decomposition used in equation (8). Also, tortuosity effects have not been specifically included but are implicit in the formalism since both $D_{iK}$ and $\kappa$ are measured quantities.

Considerable insight and confidence may be gained

regarding equations (20) and (21) by examining two interesting limits:

(1) *Single gas*

Here we put $n_2 = J_2 = 0$ to get the single equation

$$J_1 = -\frac{\phi D_{1K}}{kT}\frac{\partial p_1}{\partial z} - \frac{n_1 \kappa}{\mu}\frac{\partial p_1}{\partial z}. \tag{22}$$

Since $\kappa$ varies roughly as $R^2$, we see that for $R \to 0$ we recover the Knudsen limit

$$J_1 = -\frac{\phi D_{1K}}{kT}\frac{\partial p_1}{\partial z} \tag{23}$$

and for $R \to \infty$ we recover Darcy's law

$$v_{1D} = -\frac{\kappa}{\mu}\frac{\partial p_1}{\partial z} \tag{24}$$

where we have defined the Darcy velocity by

$$v_{1D} \equiv \frac{J_1}{n_1}. \tag{25}$$

(2) *Binary diffusion limit*

In the limit of large pore size, high porosity and low flux, we may put $\partial p/\partial z = 0$ and $\phi = 1$ in equation (20) and multiply through by $nD_{12}/D_{1K}$ to get

$$n_1 J_2 - n_2 J_1 = \frac{nD_{12}J_1}{D_{1K}} + \frac{nD_{12}}{kT}\frac{\partial p_1}{\partial z}. \tag{26}$$

As $R \to \infty$ the first term on the RHS vanishes [c.f. equation (11)] and equation (26) may be written

$$\frac{n_1 J_2 - n_2 J_1}{n^2} = D_{12}\frac{\partial}{\partial z}\left(\frac{n_1}{n}\right) \tag{27}$$

which is the standard form of the diffusion equation found in Hirschfelder, Curtiss and Bird [15] for constant total pressure and no external forces. Thus as the porous medium vanishes, the standard diffusion equation is recovered as expected.

## 3. NON-DIMENSIONALIZATION

We first wish to non-dimensionalize all quantities in equations (20) and (21). All vapor properties are normalized to the reference conditions $n_0, p_0, T_0$ which are related by

$$p_0 = n_0 k T_0. \tag{28}$$

Introducing a characteristic length $l$, we thus define

$$\tilde{n} = \frac{n}{n_0}, \tag{29}$$

$$\tilde{p} = \frac{p}{p_0}, \tag{30}$$

$$\tilde{T} = \frac{T}{T_0}, \tag{31}$$

and

$$\tilde{r} = \frac{r}{l}. \tag{32}$$

The axial variable $z$ has been replaced by $r$ since a radial pore coordinate is no longer needed. The equation of state for each component is thus

$$\tilde{p}_i = \tilde{n}_i \tilde{T}. \tag{33}$$

In addition we define

$$\tilde{J}_i = \frac{J_i l}{\phi n_0 D_{12}(p_0, T_0)}, \tag{34}$$

$$\tilde{D}_{12} = \frac{D_{12}(p, T)}{D_{12}(p_0, T_0)} \tag{35}$$

and

$$\tilde{D}_{iK} = \frac{D_{iK}(T)}{D_{iK}(T_0)}, \tag{36}$$

together with the parameters

$$\eta_i = \frac{D_{iK}(T_0)}{D_{12}(p_0, T_0)} \tag{37}$$

and

$$\xi = \frac{p_0 \kappa}{\mu \phi D_{12}(p_0, T_0)}. \tag{38}$$

Equations (20) and (21) then become

$$\tilde{J}_1 = -\eta_1 \frac{\tilde{D}_{1K}}{\tilde{T}}\frac{\partial \tilde{p}_1}{\partial \tilde{r}} - \xi \tilde{n}_1 \frac{\partial \tilde{p}}{\partial \tilde{r}} + \eta_1 \frac{\tilde{D}_{1K}}{\tilde{n}\tilde{D}_{12}}(\tilde{n}_1 \tilde{J}_2 - \tilde{n}_2 \tilde{J}_1) \tag{39}$$

and

$$\tilde{J}_2 = -\eta_2 \frac{\tilde{D}_{2K}}{\tilde{T}}\frac{\partial \tilde{p}_2}{\partial \tilde{r}} - \xi \tilde{n}_2 \frac{\partial \tilde{p}}{\partial \tilde{r}} + \eta_2 \frac{\tilde{D}_{2K}}{\tilde{n}\tilde{D}_{12}}(\tilde{n}_2 \tilde{J}_1 - \tilde{n}_1 \tilde{J}_2). \tag{40}$$

## 4. DRYING EQUATIONS

We will now specialize equations (39) and (40) to apply specifically to drying problems. Figure 2 shows a porous medium extending to the right from $\tilde{r} = 1$ in a general curvilinear geometry with an evaporation front at $\tilde{r} = \tilde{r}_f$. We replace the indices 1 and 2 by v (water vapor) and a (air) respectively. Since air cannot penetrate the front we have $\tilde{J}_a = 0$ immediately. Equations (39) and (40) then reduce to

$$\tilde{J}_v = -\eta_v \frac{\tilde{D}_{vK}}{\tilde{T}}\frac{\partial \tilde{p}_v}{\partial \tilde{r}} - \xi \tilde{n}_v \frac{\partial \tilde{p}}{\partial \tilde{r}} - \eta_v \frac{\tilde{D}_{vK}}{\tilde{n}\tilde{D}_{va}} \tilde{n}_a \tilde{J}_v \tag{41}$$

and

$$0 = -\eta_a \frac{\tilde{D}_{aK}}{\tilde{T}}\frac{\partial \tilde{p}_a}{\partial \tilde{r}} - \xi \tilde{n}_a \frac{\partial \tilde{p}}{\partial \tilde{r}} + \eta_a \frac{\tilde{D}_{aK}}{\tilde{n}\tilde{D}_{va}} \tilde{n}_a \tilde{J}_v. \tag{42}$$

If we now multiply equation (41) by $\eta_a$, equation (42) by $\eta_v$ and add, we get

$$\frac{\partial \tilde{p}}{\partial \tilde{r}} = -\frac{\tilde{J}_v}{(\eta_v/\tilde{T}^{1/2}) + \xi(\tilde{n}_v + S\tilde{n}_a)} \tag{43}$$

where we have used [c.f. equations (11), (12) and (36)]

$$\tilde{D}_{vK} = \tilde{D}_{aK} = \tilde{T}^{1/2} \tag{44}$$

and have defined

$$S \equiv \frac{\eta_v}{\eta_a} = \left(\frac{m_a}{m_v}\right)^{1/2}. \tag{45}$$

Rearranging equations (41) and using equation (44) gives

$$\frac{\partial \tilde{p}_v}{\partial \tilde{r}} = -\frac{\tilde{T}^{1/2}}{\eta_v}\tilde{J}_v - \frac{\xi \tilde{n}_v \tilde{T}^{1/2}}{\eta_v}\frac{\partial \tilde{p}}{\partial \tilde{r}} - \frac{\tilde{T}\tilde{n}_a}{\tilde{n}\tilde{D}_{va}}\tilde{J}_v. \tag{46}$$

Equations (43) and (46) are the basic working equations for drying problems. With the addition of a continuity equation, they may be solved as a two-point boundary value problem with boundary conditions

$$\left.\begin{aligned}\tilde{p} &= \tilde{p}_{amb}\\ \tilde{p}_v &= \tilde{p}_{v0}\end{aligned}\right\} \quad \text{at } \tilde{r} = 1$$

and (47)

$$\tilde{p}_v = \tilde{p}_{vap} \quad \text{at } \tilde{r} = \tilde{r}_f$$

where $p_{vap}$ is the equilibrium partial pressure of water vapor in the presence of liquid water, and $p_{amb}$ is the total pressure (usually atmospheric) at the drying surface.

The nature of equations (43) and (46) may be more fully understood by further specializing to the isothermal case $\tilde{T} = \tilde{T}_c$ in planar geometry. In that case $\tilde{J}_v = \tilde{J}_{v0}$ (a constant) is the continuity equation, and if we approximate $S$ by unity, then $\eta_a = \eta_v = \eta$ and we may obtain analytic solutions. Numerical solutions show the results to be essentially unaffected by the change from $S = 1.25$ to $S = 1$. Now equation (43) integrates directly to

$$\tilde{p} = -\frac{\eta \tilde{T}_c^{1/2}}{\xi} + \left[\left(1 + \frac{\eta \tilde{T}_c^{1/2}}{\xi}\right)^2 - \frac{2\tilde{J}_{v0}\tilde{T}_c}{\xi}(\tilde{r} - 1)\right]^{1/2} \tag{48}$$

where $\tilde{p} = 1$ has been used as the $\tilde{r} = 1$ boundary condition. The binary diffusion coefficient for air and water vapor is given by [17]

$$D_{va} = 2.302\left(\frac{p'}{p}\right)\left(\frac{T}{T'}\right)^{1.81} \times 10^{-5}\ \mathrm{m^2\,s^{-1}}$$

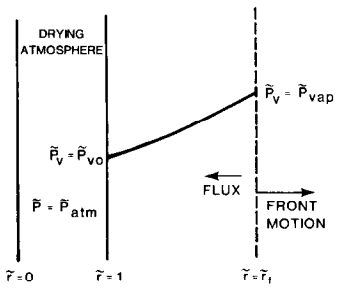


FIG. 2. Schematic of typical drying problem with boundary conditions.

where

$$p' = 0.98 \times 10^5\ \mathrm{N\,m^{-2}} \tag{49}$$
$$T' = 256\ \mathrm{K}$$

so that

$$\tilde{D}_{va} = \tilde{T}^{1.81}/\tilde{p}.$$

Then with the same approximations, equation (42) may also be integrated to yield

$$\tilde{n}_a = \frac{1}{\tilde{T}_c}\exp\left[-\frac{\xi}{\eta \tilde{T}_c^{1/2}}[\tilde{p}(\tilde{r}) - 1] + \frac{\tilde{J}_{v0}}{\tilde{T}_c^{0.81}}(\tilde{r} - 1)\right] \tag{50}$$

where $\tilde{n}_a = 1/\tilde{T}_c$ has been used at $\tilde{r} = 1$. We now analyze equations (48) and (50) in three limiting cases:

(a) *Large flux* $|\tilde{J}_{v0}| \gg 1$.

This case arises due to either high pressures $[\tilde{p}(\tilde{r}_f) \gg 1]$ or high permeabilities ($\xi \gg 1$). Since $\tilde{p}(\tilde{r}) > 1$ and $\xi$, $\eta$ are positive while $\tilde{J}_{v0}$ is negative, it follows that $\tilde{n}_a(\tilde{r})$ satisfies the inequality

$$\tilde{n}_a(\tilde{r}) < \frac{1}{\tilde{T}_c}\left[\exp\frac{\tilde{J}_{v0}}{\tilde{T}_c^{0.81}}(\tilde{r} - 1)\right]. \tag{51}$$

Thus in this case $\tilde{n}_a$ decays quickly to zero as we move into the material, i.e. most of the pore space is pure water vapor. This arises from the large flux of water vapor 'expelling' the air due to molecular collisions (binary diffusion). In this case ignoring the air component altogether, as has often been done [5, 6, 10] is a good approximation. Since the gas component at $\tilde{r} = \tilde{r}_f$ is all water vapor, we may now solve equation (48) for $\tilde{J}_{v0}$

$$\tilde{J}_{v0} = \frac{\xi}{2\tilde{T}_c(\tilde{r}_f - 1)}\left[\left(1 + \frac{\eta \tilde{T}_c^{1/2}}{\xi}\right)^2 - \left(\tilde{p}_{vap} + \frac{\eta \tilde{T}_c^{1/2}}{\xi}\right)^2\right] \tag{52}$$

When $\tilde{p}_{vap} \gg 1$ and $\xi \gg \eta$, equation (52) becomes

$$\tilde{J}_{v0} = -\frac{\xi \tilde{p}_{vap}^2}{2\tilde{T}_c(\tilde{r}_f - 1)} \tag{53}$$

which is the approximate non-dimensional form of Darcy's Law for this problem. On the other hand, if the permeability is low

$$\left(\xi \to 0, \frac{\tilde{T}_{c\eta}^{1/2}}{\xi} \gg \tilde{p}_{vap} \gg 1\right),$$

then equation (52) becomes

$$\tilde{J}_{v0} = -\frac{\eta \tilde{p}_{vap}}{\tilde{T}_c^{1/2}(\tilde{r}_f - 1)} \tag{54}$$

which is the approximate form of the Knudsen diffusion equation. The striking difference between equations (53) and (54) is the power of $\tilde{p}_{vap}$. In the Darcy flow case, the flux is proportional to $\tilde{p}_{vap}^2$, whereas for

Knudsen diffusion it is proportional to $\tilde{p}_{vap}$. Since $\tilde{p}_{vap}$ is a strong function of temperature, the two mechanisms will exhibit considerably different temperature dependences.

(b) *Knudsen limit*, $\xi \to 0$

Since $\kappa \propto R^2$ while $\eta \propto R$, as the pore size $R$ decreases, $\eta/\xi \to \infty$. In this limit we may expand equation (48) to read

$$\tilde{p} = 1 - \frac{\tilde{J}_{v0}\tilde{T}_c^{1/2}(\tilde{r}-1)}{\eta}. \tag{55}$$

Consequently in the Knudsen limit the pressure is linear with $\tilde{r}$. Note that for large $\tilde{p}$ equation (55) agrees with equation (54), but equation (55) is also valid for pressures $\tilde{p}$ approaching unity. Equation (50) becomes (for $\xi \to 0$)

$$\tilde{n}_a = \frac{1}{\tilde{T}_c}\exp[\tilde{J}_{v0}(\tilde{r}-1)\tilde{T}_c^{-0.81}]. \tag{56}$$

For large fluxes, $\tilde{n}_a$ vanishes inside the porous medium as before. However for small $\tilde{J}_{v0}$, we may expand equation (56) to give

$$\tilde{n}_a = 1/\tilde{T}_c + \tilde{J}_{v0}(\tilde{r}-1)\tilde{T}_c^{-1.81} \tag{57}$$

and using equation (55),

$$\tilde{n}_v = -\tilde{J}_{v0}(\tilde{r}-1)\left(\tilde{T}_c^{-1.81} + \frac{1}{\eta\tilde{T}_c^{1/2}}\right). \tag{58}$$

In this case the gas near the evaporation front may be nearly all air, but a simple model for Knudsen diffusion which neglects the air is still valid. This may be seen by evaluating equation (58) at $\tilde{r} = \tilde{r}_f$ with $\eta \ll 1$ (implied in the limit $\xi \to 0$) to get the Knudsen limit

$$\tilde{J}_{v0} = -\frac{\eta\tilde{p}_{vap}}{(\tilde{r}_f-1)\tilde{T}_c^{1/2}}. \tag{59}$$

(c) *Diffusion limit*

As the pore size $R$ increases at constant temperature, a point is reached where the porous medium no longer offers resistance to the moving water vapor. At that point the flux is limited by binary diffusion of water vapor through the air. We investigate this limit by taking $\xi \to \infty$ in equation (48) to get

$$\tilde{p} = 1 - \frac{\tilde{J}_{v0}\tilde{T}_c(\tilde{r}-1)}{\xi}. \tag{60}$$

It is clear from equation (60) that for large $\xi$ and moderate fluxes the pressure approaches 1 everywhere. Inserting equation (60) into equation (50) and taking $\eta \to \infty$ along with $\xi$ gives

$$\tilde{n}_a = \frac{1}{\tilde{T}_c}\exp[\tilde{J}_{v0}(\tilde{r}-1)\tilde{T}_c^{-0.81}]$$

$$\approx \frac{1}{\tilde{T}_c} + \tilde{J}_{v0}(\tilde{r}-1)\tilde{T}_c^{-1.81} \tag{61}$$

as in the Knudsen case, but now

$$\tilde{n}_v \simeq -\tilde{J}_{v0}(\tilde{r}-1)\tilde{T}_c^{-1.81} \tag{62}$$

and

$$\tilde{J}_{v0} = -\frac{\tilde{p}_{vap}\tilde{T}_c^{0.81}}{(\tilde{r}_f-1)}. \tag{63}$$

## 5. NUMERICAL SOLUTIONS FOR A STATIONARY FRONT

We now revert back to equations (43) and (46), which require numerical solution, and will compute the flux of water vapor emanating from a stationary evaporation front. We will again consider the planar isothermal case, but will allow $S$ to be the correct value (1.25 if we approximate air as being entirely $N_2$). Boundary conditions are given by equations (47) with $\tilde{p}_{v0} = 0$ (dry boundary) and $\tilde{p}_{amb} = 1$. The solution method requires an iterative procedure which starts with a guess for $\tilde{J}_{v0}$. Solutions are then obtained for $\tilde{p}_v$ and $\tilde{p}$ using a marching integration starting from $\tilde{r} = 1$, where boundary conditions are known. The resulting value of $\tilde{p}_v$ obtained at $\tilde{r} = \tilde{r}_f$ is then checked against $\tilde{p}_{vap}$ and a correction made in $\tilde{J}_{v0}$ for the next iteration. The number of iterations necessary varied from 3 for low flux problems to 50 or more for high flux problems. For concreteness in the following calculations, we will take $\phi = 0.25$, $\tilde{r}_f = 2$, $p_0 = 1$ bar ($10^5$ N m$^{-2}$) $T_0 = 300$ K (27°C), $\mu = 2 \times 10^{-5}$ kgm s$^{-1}$, and $D_{12}(p_0, T_0) = 3 \times 10^{-5}$ m$^2$ s$^{-1}$, while varying temperature and permeability. The pore size $R$ will be estimated from the capillary formula (19)

$$R = \left(\frac{8\kappa}{\phi}\right)^{1/2}. \tag{64}$$

The resulting profiles for the case $T = 70$°C ($\tilde{T} = 1.143$) are shown in Fig. 3 for permeabilities ranging from $10^{-16}$ to $10^{-13}$ m$^2$. Notice that as the permeability is raised the pressure approaches unity everywhere and thus the number density profiles approach the diffusion limit results. For this low temperature case, the gas is mostly air and in fact as we approach zero permeability (and thus zero flux) the air density approaches that of the outside atmosphere everywhere within the pores. At higher temperature (Fig. 4) the fluxes are high enough to begin pushing air from the pores until at $\kappa = 10^{-13}$ m$^2$ the gas is almost all water vapor. The behavior illustrated in Figs. 3 and 4 is basically identical to that portrayed analytically in section 4.

Next we examine the temperature dependence of the flux by plotting $\tilde{J}_{v0}$ vs $T$ for different permeabilities in Fig. 5. As the permeability is increased, the values of the flux in the regions below and above 100°C (the boiling point for this example) behave quite differently. Below 100°C, the flux saturates (as it must) to the diffusion limit which would apply if there were no porous medium at all. Above 100°C, however, there is a constant pressure gradient which, with a decreasing flow resistance, gives an increasing flux. Consequently, for permeabilities $\gtrsim 10^{-13}$ m$^2$, there is a large increase in flux as one crosses the boiling point. In fact, for $\kappa = 10^{-12}$ m$^2$ (the permeability of tight sand) a 2°C change

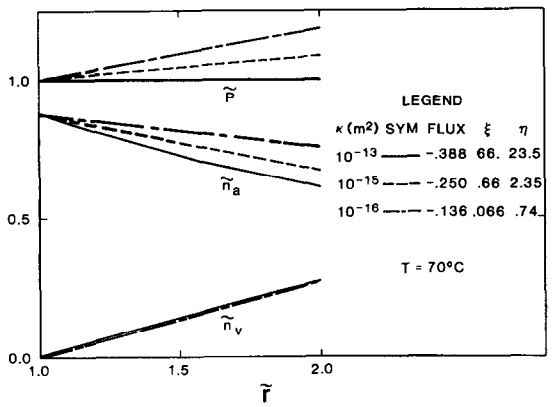


FIG. 3. Density and pressure profiles for an isothermal drying problem at 70°C. $\tilde{r} = 2$ is the evaporation front position.

in temperature at 100°C gives an order of magnitude increase in flux. This result corresponds with the intuitive notion of 'boiling', and is commonly invoked in calculations by assuming a vapor region boundary which follows the boiling temperature. However, as we approach values of $\kappa$ in the range $\lesssim 10^{-15}$ m$^2$ (the permeability of many common rocks, including tuffs, granite, etc.), we see that no abrupt change occurs at 100°C. This is because for low permeabilities the flux is not diffusion limited below 100°C, and consequently the character of the vapor transport remains the same as the boiling temperature is crossed, i.e. forced flow. It therefore follows that calculations involving low permeability saturated materials above the boiling point should be done using a correct vapor transport model. Furthermore, for such problems the evaporation front (if there is one) will not necessarily follow the boiling isotherm.

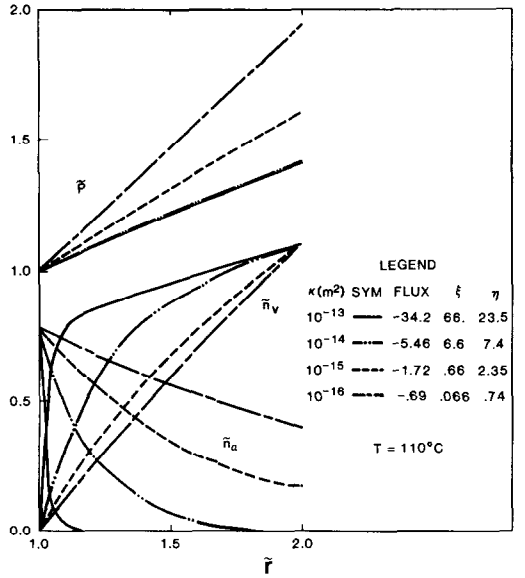


FIG. 4. Density and pressure profiles for an isothermal drying problem at 110°C. $\tilde{r} = 2$ is the evaporation front position.

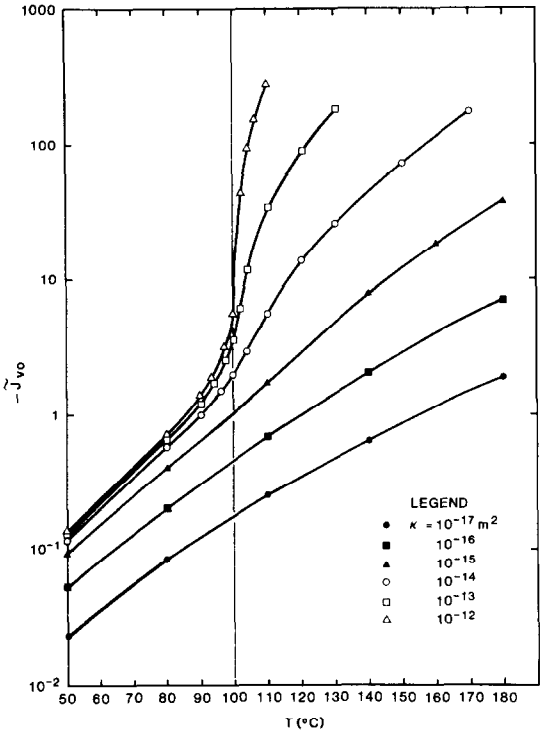


FIG. 5. Flux of water vapor from a stationary evaporation front vs. sample temperature (uniform).

## 6. EVAPORATION FRONT MOTION

We now turn our attention from the detailed transport mechanisms in the vapor region to the motion of the evaporation front itself. Since in this paper motion of the liquid phase is not being considered, the front moves only when the liquid changes phase, i.e. evaporates. Mass balance at the front thus gives the following simple formula for the front velocity $u$:

$$u = -\frac{J_v m_v}{\phi \rho_l}. \tag{65}$$

This non-dimensionalizes to

$$\tilde{u} = -\gamma \tilde{J}_v \tag{66}$$

with

$$\gamma = n_0 D_{12}(p_0, T_0) m_v / \alpha_v \rho_l \tag{67}$$

where $\alpha_v$ is the thermal diffusivity to be introduced later in connection with the heat equation.

If we assume that vapor motion proceeds on a time scale short compared with front motion ($v_v \gg u$), then the water vapor flux $\tilde{J}_v$ obeys the steady state continuity equation in 1-dim.

$$\frac{1}{\tilde{r}^m}\frac{\partial}{\partial \tilde{r}}\left(\tilde{r}^m \tilde{J}_v\right) = 0 \tag{68}$$

where $m$ is the geometry indicator

$$m = \begin{cases} 0, & \text{planar,} \\ 1, & \text{cylindrical,} \\ 2, & \text{spherical.} \end{cases}$$

Solutions to equation (68) are

$$\tilde{J}_v \tilde{r}^m = \tilde{J}_{v0} \tag{69}$$

where $\tilde{J}_{v0}$ is constant in space but varies with time through its dependence on the front position $\tilde{r}_f$. Combining equations (66) and (69) gives an equation of motion for $\tilde{r}_f$

$$\frac{d\tilde{r}_f}{d\tilde{t}} = -\frac{\gamma \tilde{J}_{v0}(\tilde{r}_f)}{\tilde{r}_f^m}. \tag{70}$$

We may determine the form of $\tilde{J}_{v0}(\tilde{r}_f)$ for the case of constant temperature by returning to the derivation of the approximate equations (48) and (50). In these equations the term $\tilde{J}_{v0}(\tilde{r} - 1)$ was obtained by integrating $\tilde{J}_{v0}$ over the interval 1 to $\tilde{r}$. We may generalize this procedure by replacing $\tilde{J}_{v0}$ by $\tilde{J}_{v0}/r^m$ [equation (69)] and repeating the integral to get

$$\int_1^{\tilde{r}} \frac{\tilde{J}_{v0}}{\tilde{r}^m} d\tilde{r} = \tilde{J}_{v0} \times \begin{cases} \tilde{r} - 1 & m = 0 \\ \ln\tilde{r} & m = 1 \\ 1 - \dfrac{1}{\tilde{r}} & m = 2. \end{cases} \tag{71}$$

Notice that equation (48) evaluated at $\tilde{r} = \tilde{r}_f$ shows dependence on $\tilde{r}_f$ only in the term $\tilde{J}_{v0}(\tilde{r}_f - 1)$ since $\tilde{p}(\tilde{r}_f) = \tilde{p}_{vap}$. Thus in equations (53), (54), (59) and (63), we may replace $\tilde{J}_{v0}(\tilde{r}_f - 1)$ with the expressions in equations (71) evaluated at $\tilde{r} = \tilde{r}_f$, so that regardless of the dominant transport mechanism involved,

$$\tilde{J}_{v0}(\tilde{r}_f) = C \times \begin{cases} (\tilde{r}_f - 1)^{-1} & m = 0 \\ (\ln\tilde{r}_f)^{-1} & m = 1 \\ \left(1 - \dfrac{1}{\tilde{r}_f}\right)^{-1} & m = 2. \end{cases} \tag{72}$$

Here $\tilde{r}_f = 1$ represents the position of the drying surface and $C$ depends on temperature, $\xi, \eta$, etc. but not on $\tilde{r}_f$ or $\tilde{t}$.

There are now two classes of problems to solve which we will denote exterior and interior evaporation. In the former case, an object of finite size is dried from the outside; in the latter case (interior), an infinite domain with a finite sized cavity is dried from the inside out. Of course, the case $m = 0$ is neither exterior nor interior. We now present solutions to equations (70) and (72) for the five cases

(a) m = 0

$$\tilde{r}_f = 1 + (-2\gamma C\tilde{t})^{1/2} \tag{73}$$

and

$$\tilde{J}_{v0} = -\left(\frac{-C}{2\gamma\tilde{t}}\right)^{1/2}. \tag{74}$$

Notice that in this case the flux decays with time as $\tilde{t}^{-1/2}$ as the front erodes farther into the material.

(b) *Exterior evaporation*, m = 1

This case is that of an infinitely long cylinder dried from the outside. Here $\tilde{J}_{v0} > 0, C < 0$ and we have the implicit result

$$\tilde{r}_f = \left(\frac{1 + 4\gamma C\tilde{t}}{1 - 2\ln\tilde{r}_f}\right)^{1/2} \tag{75}$$

and

$$\tilde{J}_{v0} = \frac{C}{\ln\tilde{r}_f}. \tag{76}$$

Since $\tilde{r}_f < 1$, $\tilde{J}_{v0}$ decays quickly as the front approaches the origin.

(c) *Exterior evaporation*, m = 2

This is the case of a sphere dried from the outside. Again $\tilde{J}_{v0} > 0, C < 0$ and the front position is found by solving the cubic equation

$$2\tilde{r}_f^3 - 3\tilde{r}_f^2 + 1 = -6\gamma C\tilde{t} \tag{77}$$

with

$$\tilde{J}_{v0} = \frac{C}{\left(1 - \dfrac{1}{\tilde{r}_f}\right)}. \tag{78}$$

Again $\tilde{J}_{v0}$ decreases dramatically as $\tilde{r}_f \to 0$.

(d) *Interior evaporation*, m = 1

Here we have drying from an infinitely long cylindrical cavity of radius $\tilde{r} = 1$ into an infinite medium. Now $\tilde{J}_{v0} < 0$, and the equations are identical in form to (b) above

$$\tilde{r}_f = \left(\frac{1 + 4\gamma C\tilde{t}}{1 - 2\ln\tilde{r}_f}\right)^{1/2} \tag{79}$$

and

$$\tilde{J}_{v0} = \frac{C}{\ln\tilde{r}_f}. \tag{80}$$

Although equation (79) is not useful near $\ln\tilde{r}_f = 1/2$, we see that for long times both $\tilde{r}_f$ and $\tilde{J}_{v0}$ decay somewhat slower than the $m = 0$ case.

(e) *Interior evaporation*, m = 2

This case corresponds to drying from a spherical cavity of radius $r = 1$ into an infinite medium. We have $J_{v0} < 0$, $C < 0$ and $r_f$ is determined from [same equations as (b)]

$$2\tilde{r}_f^3 - 3\tilde{r}_f^2 + 1 = -6\gamma C\tilde{t} \tag{81}$$

with

$$\tilde{J}_{v0} = \frac{C}{\left(1 - \frac{1}{\tilde{r}_f}\right)}. \tag{82}$$

We see that for long times

$$\tilde{r}_f \simeq (-3\gamma C\tilde{t})^{1/3} \tag{83}$$

and

$$\tilde{J}_{v0} \simeq C. \tag{84}$$

The latter two cases are particularly relevant to problems arising from the disposal of nuclear waste in geologic formations, since a heat-producing waste canister is implanted into small cavity within a larger formation. The water-bearing rock may then dry with an evaporation front moving outwards from the canister. Equations (80) and (84) imply that, for a cylindrical cavity, the flux will initially decay somewhat slower than the planar case until the front is sufficiently far away from the canister. At that point since the cavity is of finite length, the problem may become more spherical than cylindrical. The flux of vapor into the hole may then approach a constant [equation (84)]. This effect arises from purely geometrical considerations, since the evaporation front area grows as the front recedes. A nearly saturating flux apparently related to the above theory has recently been seen in a heater test in tuff [18].

## 7. RESULTS FOR NON-ISOTHERMAL TRANSIENT PROBLEMS

We now lift the isothermal restriction and solve the full set of equations (43), (46), (47) and (70) together with the heat equation. The primary motivation for doing this is to study the motion of the evaporation front relative to that of various isotherms.

Denoting the vapor region ($r < r_f$) by v and the liquid region ($r > r_f$) by l, and assuming a constant conductivity in each region, the heat equation for the matrix plus vapor is

$$\frac{\partial T}{\partial t} = \frac{\alpha_v}{r^m}\frac{\partial}{\partial r}\left(r^m \frac{\partial T}{\partial r}\right) \tag{85}$$

and that for the matrix plus liquid water is

$$\frac{\partial T}{\partial t} = \frac{\alpha_l}{r^m}\frac{\partial}{\partial r}\left(r^m \frac{\partial T}{\partial r}\right). \tag{86}$$

The matching condition at the evaporation front is

$$k_l \frac{\partial T}{\partial r}\bigg|_l - k_v \frac{\partial T}{\partial r}\bigg|_v = -LJ_v m_v \tag{87}$$

where the $k$'s are effective thermal conductivities of matrix plus fluid and $L$ is the latent heat of vaporization. Equations (85) and (86) non-dimensionalize to

$$\frac{\partial \tilde{T}}{\partial \tilde{t}} = \frac{1}{\tilde{r}^m}\frac{\partial}{\partial \tilde{r}}\left(\tilde{r}^m \frac{\partial \tilde{T}}{\partial \tilde{r}}\right) \tag{88}$$

in the vapor region and

$$\frac{\partial \tilde{T}}{\partial \tilde{t}} = \left(\frac{\alpha_l}{\alpha_v}\right)\frac{1}{\tilde{r}^m}\frac{\partial}{\partial \tilde{r}}\left(r^m \frac{\partial \tilde{T}}{\partial \tilde{r}}\right) \tag{89}$$

in the liquid region. Here we have defined

$$\tilde{t} = \frac{\alpha_v t}{l^2}. \tag{90}$$

The matching condition is

$$\frac{\partial \tilde{T}}{\partial \tilde{r}}\bigg|_l - \left(\frac{k_v}{k_l}\right)\frac{\partial \tilde{T}}{\partial \tilde{r}}\bigg|_v = -\delta \frac{\tilde{J}_{v0}}{\tilde{r}^m}, \tag{91}$$

where

$$\delta = \frac{L\phi D_{va}(p_0, T_0)n_0 m_v}{k_l T_0}. \tag{92}$$

Numerical solution of the above equations on a finite difference grid begins with a determination of the flux $\tilde{J}_{v0}$ for some initial evaporation front position. Consistent with assumption (7) in section 1, this is accomplished in the same manner as for a stationary front, as was detailed in section 5. The temperature field is next advanced in time using a fully implicit space-centered scheme which incorporates the matching condition (91) at the first mesh point below the evaporation front position. The time step is completed by explicitly advancing the evaporation front position according to (70). For sufficiently small time steps, it may be shown that the order of the above calculations is immaterial.

Next we present solutions of the entire suite of equations for a selection of problems of interest. For all calculations in this section we will use $L = 2.253 \times 10^6$ J kg$^{-1}$, $k_l = k_v = 1.5$ W m$^{-1}$ K$^{-1}$, $\alpha_l = \alpha_v = 5.1 \times 10^{-7}$ m$^2$ s$^{-1}$ and $\rho_w = 1000$ kg m$^{-3}$ (the values for $k$ and $\alpha$ are for welded tuff). Thus we have $\delta = 0.028$ and $\gamma = 0.044$.

The first problem is that of a front initially at $\tilde{r} = 1$ moving in the positive $\tilde{r}$ direction. The temperature is initially set at $\tilde{T} = 1$ (300 K) and at $\tilde{t} = 0$ the boundary temperature at $\tilde{r} = 1$ is raised to $\tilde{T} = 1.277$ (383 K) and held there. Figure 6 shows isotherm and evaporation front position vs time for the planar case with $\kappa = 10^{-16}$ m$^2$. Notice that the evaporation front temperature remains constant to good accuracy. This is consistent with the assumptions of many authors, [8, 9, 10, 19] that the front follows an 'evaporation temperature' isotherm. This phenomenon arises somewhat accidentally, since for this particular temperature boundary condition and geometry, $\tilde{r}/\tilde{t}^{1/2}$ is a similarity variable [17] and the evaporation front also follows a $\tilde{t}^{1/2}$ law. This result is contrasted in Fig. 7, where the same calculation in spherical coordinates shows the evaporation front crossing isotherms. In this case the isotherms move more slowly than does the evaporation front due to the spherical geometry.

One other case where the front follows an isotherm occurs when the permeability is large and the isotherms propagate quickly into the medium. Here the

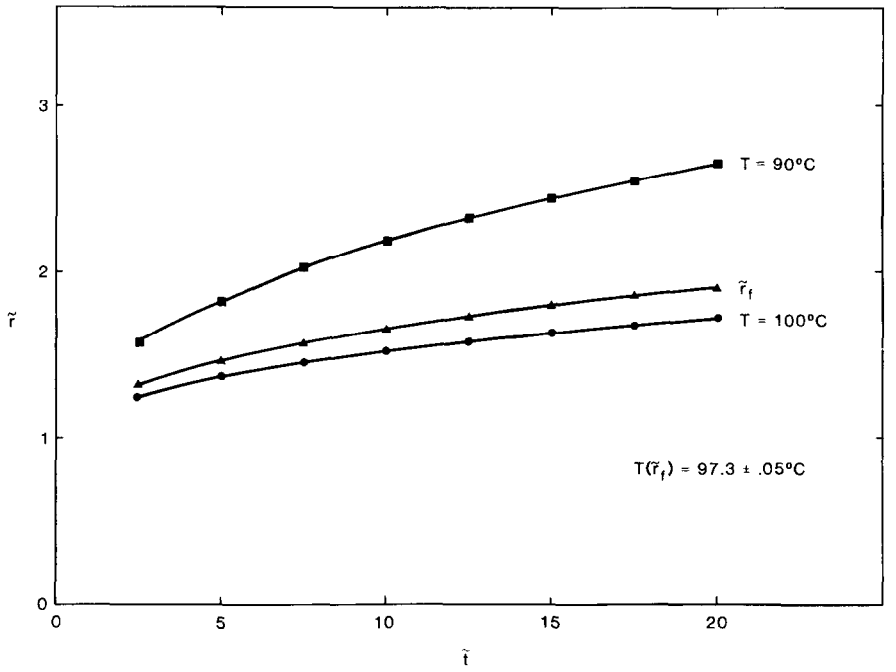


FIG. 6. Isotherm and evaporation front position vs time. Planar case with $\kappa = 10^{-16}\,m^2$.

evaporation front stays at or near the boiling point, as shown in Fig. 8. This run is for spherical geometry where it was seen in Fig. 7 that the front is normally non-isothermal. Figure 8 shows results for $\kappa = 10^{-12}\,m^2$ and a high heat flux boundary condition, and the large slope of flux vs temperature (see Fig. 5) causes the front to oscillate stably around a temperature near the boiling point; for if the front were to outrun the isotherm, a drastic reduction in flux and front velocity would occur, allowing the isotherm to catch up. Similarly, the isotherm cannot far outrun the evaporation front without the large increase in flux allowing the front to catch up. Even at high permeability, however, this condition will not occur unless the boiling isotherm is being driven into the material faster than the front tends to recess.

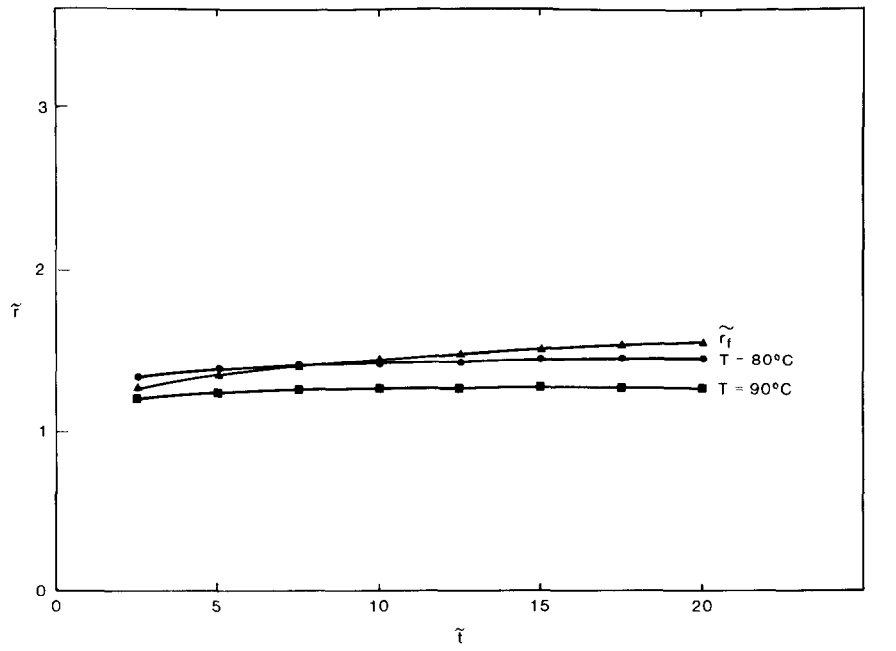


FIG. 7. Isotherm and evaporation front position vs time. Spherical case with $\kappa = 10^{-16}\,m^2$.

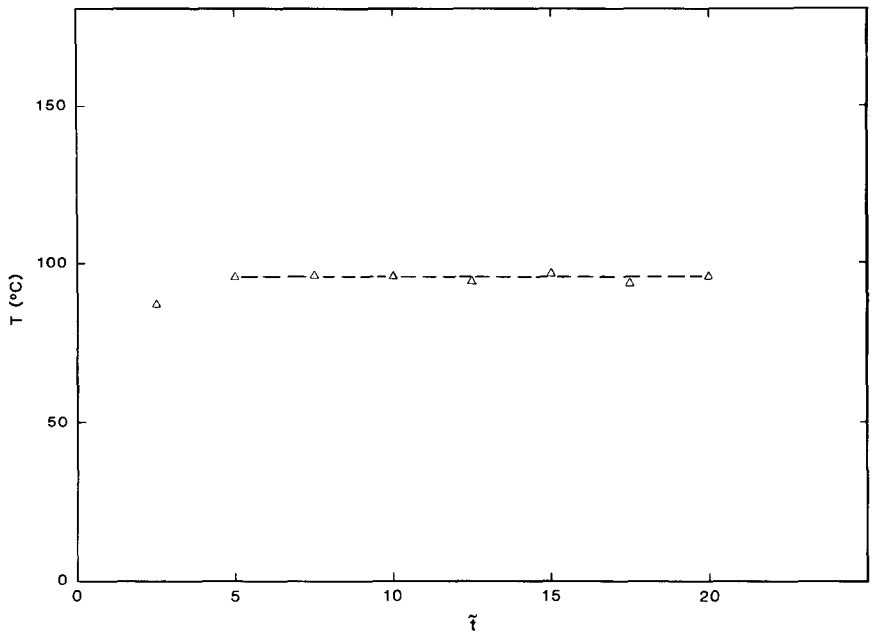


FIG. 8. Isotherm and evaporation front position vs time. Spherical case with high heat flux boundary condition and $\kappa = 10^{-12}\,m^2$.

## 8. CONCLUSION

A formalism has been presented for the solution of evaporation front drying problems. The formalism is kinetic theory-based and includes both diffusion and viscous flow of a binary gas mixture through a porous medium. Previous simple treatments which ignore the presence of air in the pores are recovered as limits of the more general theory and are shown to be valid approximations in certain cases.

Solutions presented of water vapor flux versus temperature for a stationary front show that the concept of 'boiling' is of limited usefulness for materials of low permeability (below $10^{-14}\,m^2$), while still retaining its normal interpretation for high permeability materials. This is important for heat transfer calculations done on tight saturated geological materials in which the boiling point is exceeded, and demonstrates that for these cases the assumption of vapor only for regions with temperatures above the boiling point may not be valid.

When the motion of the evaporation front is included toether with sample constant temperature solutions for the vapor region, useful information is obtained concerning the effect of geometry on the water loss rate. The latter decreases proportional to $t^{-1/2}$ for the planar case, and for drying occurring from a cavity, more slowly in cylindrical geometry, until for spherical geometry it approaches a constant. This occurs because the area of the evaporation front increases to compensate for the lower flux as the front propagates into the material. This result is significant and indicates that a dried spherical cavity in an infinite medium will, after a certain period of time, develop a water inflow rate which remains constant indefinitely.

Finally, solutions are presented for the motion of isotherms and evaporation fronts for a transient drying problem with the heat equation included. Although the planar case (with an initially constant temperature suddenly raised and then held constant at the drying boundary) shows an isothermal evaporation front, this is not true as a general rule. Other calculations done in spherical geometry or with other boundary conditions on temperature show that the evaporation does not stay at an 'evaporation temperature' but in general crosses isotherms.

*Acknowledgement*—This article was sponsored by the U.S. Department of Energy under Contract DE-AC04-76-DP00789.

## REFERENCES

1. E. Buckingham, Studies in the movement of soil moisture, *U.S. Dept. Agr. Bur. Soils. Sull.* **38**, 29–61 (1907).
2. N. H. Ceaglske and O. A. Hougen, Drying granular solids, *Ind. Engng Chem.* **29**, 805–813 (1937).
3. Y. K. Sherwood, Application of the theoretical diffusion equations to the drying of solids, *Trans. Am. Inst. Chem. Engrs* **27**, 190–202 (1931).
4. C. L. D. Huang, H. H. Siang and C. H. Best, Heat and moisture transfer in concrete slabs, *Int. J. Heat Mass Transfer*, **22**, 257–266 (1979).
5. R. D. Gibson, M. Cross and R. W. Young, Pressure gradients generated during the drying of porous shapes, *Int. J. Heat Mass Transfer*, **22**, 827–830 (1979).
6. J. J. Hohlfelder and G. R. Hadley, Laboratory studies of water transport in rock salt, *Lett. Heat Mass Transfer* **6**, 271–279 (1979).
7. O. A. Hougen, H. J. McCauley and W. R. Marshall, Jr., Limitations of diffusion equations in drying, *Trans. Am. Inst. Chem. Engrs* **36**, 183–210 (1940).

8. L. N. Gupta, An approximate solution of the generalized Stefan's problem in a porous medium, *Int. J. Heat Mass Transfer*, **17**, 313–321 (1974).
9. M. D. Mikhailov, Exact solution of temperature and moisture distributions in a porous half-space with moving evaporation front, *Int. J. Heat Mass Transfer* **18**, 797–804 (1975).
10. M. Cross, R. D. Gibson and R. W. Young, Pressure generation during the drying of a porous half-space, *Int. J. Heat Mass Transfer*, **22**, 47–50 (1979).
11. R. B. Evans, III, G. M. Watson and E. A. Mason, Gaseous diffusion in porous media at uniform pressure, *J. Chem. Phys.* **35**, 2076–2083 (1961).
12. R. B. Evans, III, G. M. Watson and E. A. Mason, Gaseous diffusion in porous media II. Effect of pressure gradients, *J. Chem. Phys.* **36**, 1894–1902 (1962).
13. E. A. Mason, R. B. Evans, III and G. M. Watson, Gaseous diffusion in porous media III. Thermal transpiration, *J. Chem. Phys.* **38**, 1801–1826 (1963).
14. E. A. Mason, A. P. Malinauskas and R. B. Evans, III, Flow and diffusion of gases in porous media, *J. Chem. Phys.* **46**, 3199–3216 (1967).
15. J. O. Hirschfelder, C. F. Curtiss, R. B. Bird, *Molecular theory of gases and liquids*, p. 516–517. Wiley, New York (1954).
16. G. R. Youngquist, Diffusion and flow of gases in porous solids, *Ind. Eng. Chem.* **62**, 52–63 (1970).
17. E. R. G. Eckart and R. M. Drake, Jr., *Analysis of Heat and Mass Transfer*, p. 787. McGraw-Hill (1972).
18. J. K. Johnstone and K. Wolfsbert, Sandia National Laboratories Report, SAND80-1464, p. 83 (1980).
19. S. H. Cho, An exact solution of the coupled phase change problem in a porous medium, *Int. J. Heat Mass Transfer* **18**, 1139–1142 (1975).

## TRAITEMENT THEORIQUE DE L'EVAPORATION. FRONT DE SECHAGE

**Résumé**—On présente un formalisme pour l'écoulement forcé et la diffusion d'un mélange binair gazeux à travers un milieu poreux. Les équations sont privilégiées pour traiter la région de vapeur d'un matériau poreux en cours de séchage avec un modèle de front d'évaporation. On présente des solutions pour différentes perméabilités et températures ; elles donnent les conditions pour lesquelles l'air est présent dans les pores et elles permettent d'étudier l'utilité du concept "d'ébullition" pour le séchage de matériaux faiblement perméables. Le mouvement du front d'évaporation et la perte en eau sonte examinés pour différentes géométries curvilignes, à la fois analytiquement et numériquement.

## THEORETISCHE ABHANDLUNG ÜBER DIE VERDUNSTUNGSFRONT BEI DER TROCKNUNG

**Zusammenfassung**—Es wird ein allgemeines Verfahren für kombinierte Diffusion und erzwungene Strömung eines binären Gasgemisches durch ein poröses Medium beschrieben. Die erhaltenen Gleichungen werden dann spezialisiert, damit sich der Dampfbereich des porösen Mediums behandeln läßt, das entsprechend dem Modell einer zurückweichenden Verdunstungsfront austrocknet. Die Lösungen für verschiedene Durchlässigkeiten und Temperaturen zeigen die Bedingungen auf, unter denen sich Luft in den Poren befindet, und erlauben es, die Anwendbarkeit des "Siede"-Konzepts auf die Trocknung von wenig druchlässigen Materialien zu beurteilen. Bewegungen der Verdunstungsfront und Wasserverlustrate werden sowohl analytisch als auch numerisch für verschiedene gekrümmte Geometrien untersucht.

## ТЕОРЕТИЧЕСКОЕ ИССЛЕДОВАНИЕ ПРОЦЕССА СУШКИ ПРИ ЗАГЛУБЛЕНИИ ФРОНТА ИСПАРЕНИЯ

**Аннотация**—Предложен общий математический формализм для описания одновременных процессов диффузии и вынужденного течения смеси бинарного газа через пористую среду. Полученные уравнения затем используются для описания течения пара в пористом материале, сушка которого проводится в соответствии с моделью заглубления фронта испарения. Решения, полученные для различных значений проницаемостей и температур, позволяют определить условия, при которых в порах присутствует воздух, что дает возможность рассматривать применимость понятия "кипение" к сушке материалов с малой проницаемостью. Аналитически и численно исследуются перемещение фронта испарения и интенсивность испарения воды для различных криволинейных геометрий.